applied sciences

MDPI

Brief Report

Low-Cost Microwave Sensor for Characterization and Adulteration Detection in Edible Oil

Muhammad Hamza Bhatti, Muhammad Abdul Jabbar, Muhammad Atif Khan and Yehia Massoud *

Innovative Technologies Laboratories (ITL), King Abdullah University of Science and Technology (KAUST), Thuwal 23955, Saudi Arabia
* Correspondence: yehia.massoud@kaust.edu.sa

Featured Application: Characterization of liquids especially edible oils and adulteration detection using dielectric spectroscopy.

Abstract: A low-cost microwave sensor was designed for oil adulteration detection and characterization of pure edible oil using dielectric spectroscopy. The sensor's final design was fabricated on a low cost 1.6 mm thick FR-4 substrate with a combination of a complementary split ring resonator and a transmission line. The sensor's dimensions were 35 × 30 × 1.6 mm^3 with a substrate dielectric constant of 4.3. A 5.25 GHz resonance frequency was selected as a reference for characterization and adulteration detection in pure edible oil. Initially, pure olive, caster, flaxseed, and mustard oil were characterized by the design sensors, with frequency shifts of 250, 370, 150, and 320 MHz, respectively. Pure olive oil with adulteration of castor, mustard, and argemone oil, was tested by placing the samples directly on the sensor. The experimental results showed that the sensor can detect 10% to 30% adulteration in the olive oil. The maximum sensitivity, frequency shift and quality factor were noted as 4.6, 530 MHz and 39, respectively. The high values of sensitivity and quality factor, along with agreement between simulated and experimental results, makes our sensor a good candidate for oil characterization and adulteration detection.

Keywords: microwave sensor; dielectric spectroscopy; complementary split ring resonator; adulteration detection

Citation: Bhatti, M.H.; Jabbar, M.A.; Khan, M.A.; Massoud, Y. Low-Cost Microwave Sensor for Characterization and Adulteration Detection in Edible Oil. *Appl. Sci.* **2022**, *12*, 8665. https://doi.org/10.3390/app12178665

Academic Editor: Ernesto Limiti

Received: 1 August 2022
Accepted: 25 August 2022
Published: 29 August 2022

1. Introduction

The importance of sensors is undeniable in today's world of technology and innovation. The advent of the Internet of Things and automation has raised their significance to unprecedented levels [1]. With advancements in the areas of electronics, photonics and materials, new types of sensors are introduced every year [2–8]. Recent research has focused on developing sensors with high accuracy, compact size and high sensitivity [9–15]. Microwave sensors employ an electromagnetic field for sensing purposes, and operate in a frequency range of 300 MHz to THz [1]. Microwave sensors have several advantages over their counterparts including low cost, compact size, accuracy, ease of fabrication, and testing [16–21]. Due to these obvious advantages, microwave sensors play a vital role in different fields of life such as healthcare, agriculture, the defense sector, and industry [9–11,22–24]. Microwave sensors can be categorized into two types: (i) broadband sensors, and (ii) resonance-based sensors. Resonance-based sensors operate on a narrow frequency range with high precision [10] and utilize a highly confined and dense electric field for sensing. The resonance frequency is extremely sensitive to dielectric loading in this region, and any minute change can result in a shift in resonance frequency. The use of metamaterial structures such as split rings (SRR) or complementary split rings (CSRR) in microwave sensors has further enhanced the accuracy of measuring dielectric permittivity [25–28]. Furthermore, different oil molecules have different rotational dynamics and correlation times, and can achieve resonance with the applied external electric field at different frequencies.

The detection of adulteration in food has remained a key application of microwave sensors. For example, the purity of edible oils plays an important role in human health. Contamination in edible oils could be due to intentional adulteration, or as a result of factors such as aging or improper packing. Adulterated oil can harm human health by causing different types of diseases, such as cardiovascular and throat diseases [29]. Dielectric spectroscopy using microwave sensors has been widely employed to detect adulteration in edible oils. Cavity resonator-based sensors for liquid characterization have been reported in the literature [30]. However, planar microwave sensors are preferred over large bulky cavity resonators due to advantages such as low cost, easy use, easy fabrication, and the benefits of integration with other microwave devices. A high-sensitivity sensor with a non-destructive technique for the detection of complex permittivity of liquids was presented in [31]. The sensor was mounted on a Rogers RT6002 substrate and the sample testing was carried out inside a polydimethiolsilicon (PDMS) microchannel. High sensitivity was achieved by incorporating only a single capacitor in the LC resonator circuit. A CSRR-based planar microwave sensor for adulteration detection in edible oils was proposed in [32]. This sensor was designed on a Roger 5880 substrate and could detect adulteration of up to 20%. The sensor presented in [33] employed a resonator on FR4 substrate to detect adulteration in oils, but the sensitivity and quality factors of the proposed sensor were not calculated. These two parameters are the most crucial parameters to determine the performance of a sensor. In [34], the proposed sensor could detect oil adulteration only in the range of 50% and above. One of the drawbacks in the existing literature includes the use of expensive substrates such as Rogers, which will become critical at the mass production stage. Sensors fabricated on low-cost substrates have either low sensitivity, or cannot detect low levels of adulteration. Moreover, the use of the PDMS microchannel also makes the testing process complicated. In this paper, we present a highly sensitive low-cost CSRR-based microwave sensor for adulteration detection in, and characterization of, edible oil. The sensor was simulated on Computer Simulation Technology (CST) Microwave Studio and fabricated on commercially available low-cost FR-4 substrate. The sensor could measure the complex permittivity of an unknown oil by the resonance frequency and peak attenuation, which can also be used to identify the unknown oil. Two empirical equations were developed to calculate the permittivity and loss tangent of unknown oils from the shift in resonance frequency and peak attenuation. The sensor operated at a frequency of 5.25 GHz with maximum sensitivity and quality factor of 4.6 and 39, respectively. The proposed sensor possessed advantages such as low cost, compact design, ease of fabrication and high sensitivity. Later sections will extensively discuss the design, simulation, experimental results, and validation.

2. Design and Simulation

Most transmission line-based structures are based on changes in electric and magnetic fields. The electric field plays an important role in the characterization of edible oil samples. Oil samples are placed directly on the sensor so the electric field can easily contact the CSRR. Ideally, the introduction of pure dielectric oil should not affect the inductance of the sensor. Only the sensor's overall capacitance is altered by the placement of oil samples on the sensing zone, with the outcome that the sensor's resonating frequency is shifted. This change in resonant frequency is attributed to the real part of permittivity of the oil under test (OUT). The top and bottom views of the proposed sensor with all the dimensions are shown in Figure 1. A four square CSRR structure was etched in the ground plane, whereas the top surface consisted of a feeding transmission line only. When the electromagnetic wave was fed, the rings induced a magnetic field and acted as an inductor, whereas the split gap acted as a capacitor. The combined effect of capacitance and inductance determined the resonance frequency, at which the sensor behaved as a narrow band stop filter. Using a time domain solver, the sensor was designed on a low-cost FR-4 substrate in CST Microwave

Studio. The sensor's dimensions were optimized in CST Microwave Studio to obtain a confined electric field and a resonance frequency of 5.20 GHz, as shown in Figure 1.

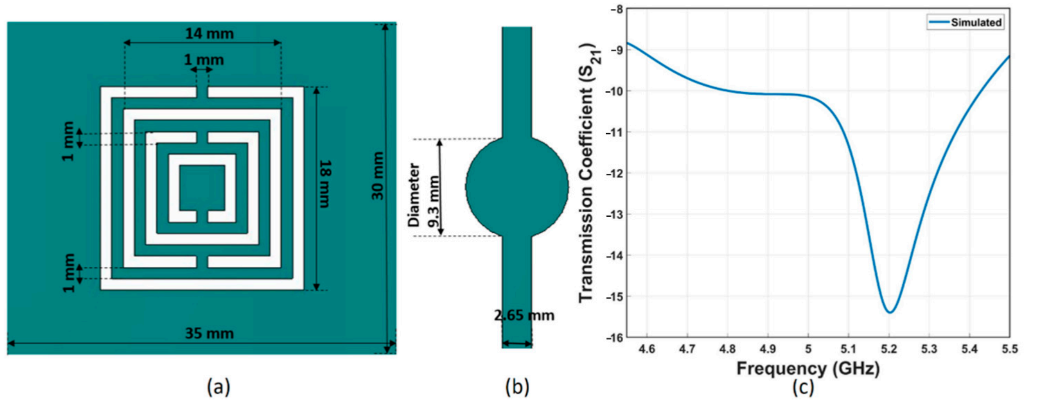

Figure 1. (**a**) Four-ring resonator in the ground plane of the sensor. (**b**) Feed line of sensor. (**c**) Transmission coefficient (S_{21}) at different frequencies.

In the design, a two port network was used to feed the sensor, such that the input was provided at port 1 and output was measured at port 2, using National Instruments Vector Network Analyzer (NI—VNA). When the electromagnetic wave was transmitted from port-1, most energy was stored in the CSRR at resonance. This energy then interacted with OUT and shifted the resonance frequency. The transmission coefficient (S_{21}) was used to estimate the resonance frequency. The ports were connected with CSRR in the ground plane and had an impedance of 50 Ω. The ground plane was designed in such a way so that 50 Ω impedance was matched. The simulated result for the forward transmission coefficient (S_{21}) is shown in Figure 1.

The equivalent circuit model for our CSRR was extracted using the techniques presented in [35]. The equivalent circuit model is shown in Figure 2b and was used to calculate the dimensions required to operate the sensor on the desired resonating frequency. The resonance frequency of the circuit presented in Figure 2b was calculated by Equation (1), and it matched well with the resonance frequency of our CSRR. In Equation (1), *L* and *C* are equivalent inductance and capacitance of CSRR, respectively.

$$f_r = \frac{1}{2\pi\sqrt{LC}} \tag{1}$$

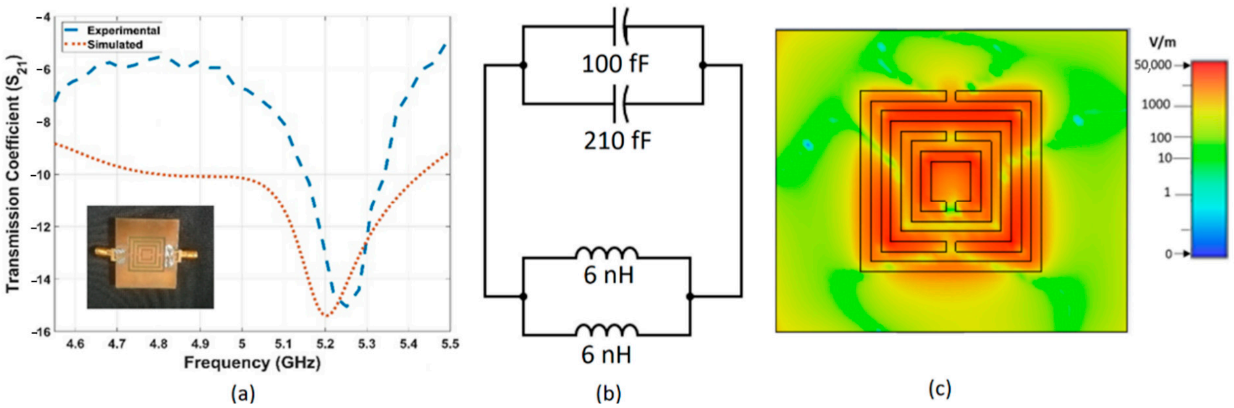

Figure 2. (**a**) Simulated and experimental values of transmission coefficient (S_{21}) at different frequencies. (**b**) Equivalent LC model of the CSRR sensor. (**c**) Electric field profile at the resonance frequency.

Figure 2c presents the electric field profile of the resonator at the resonance frequency, and a concentrated electric field can be seen in the ground plane in the region of CSRR.

This region of the high electric field was utilized for detection because this region had the highest sensitivity to changes in the dielectric permittivity.

3. Experimental Results and Validation

3.1. Device Fabrication

Keeping in mind the research aims of low cost, ease of fabrication, good quality factor, and improved sensitivity, the sensor was fabricated on an FR-4 substrate with a dielectric constant of 4.3. The fabricated sensor with the experimental measurement setup is shown in Figure 3. The sensor width was 30 mm and the length was 35 mm. The SMA connectors were manually soldered to feed the sensor. Oil samples were directly placed on the sensor's high sensitive electric field area for characterization and adulteration detection of different oil samples.

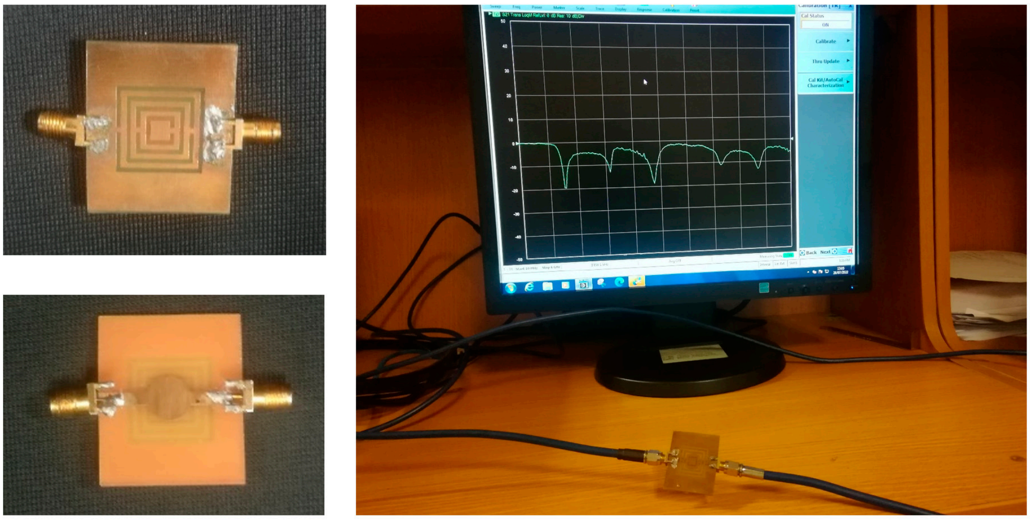

(a) (b)

Figure 3. (**a**) Front and back picture of the fabricated sensor. (**b**) Experimental set-up used for oil testing.

3.2. Dielectric Characterization of Oil Samples

The comparison of simulation and experimental results of the scattering parameters of the unloaded sensor is shown in Figure 2a. The simulated and measured S_{21} showed the sensor resonating at 5.20 GHz and 5.25 GHz, respectively. The forward transmission coefficient was measured to check the resonant frequency, and as seen in Figure 2, the simulated and experimental results were close enough. The slight shift in resonance frequency was attributed to the fabrication tolerance. Before adulteration detection, the sensor was tested by measuring the permittivity values of some commonly available oils. Castor oil, mustard oil, flaxseed oil, and olive oil samples were used to experiment with dielectric characterization. The oils are commonly available and were bought from a supermarket. To calculate the complex permittivity of the different oil samples, a unique empirical formula is required [33]. Equations (2) and (3) were used to calculate the real part of the permittivity and loss tangent of the oil samples. Each oil sample had a different resonating frequency, and using the shift in resonating frequency compared with the unloaded sensor, characterization of the oil samples took place.

$$\epsilon_r = \frac{-1}{0.19083} \ln \frac{(\Delta f - 1.75477)}{-2.10315} \tag{2}$$

$$\tan\delta = \frac{-1}{-0.2687 - 3.32877\epsilon_r + 0.54996(\epsilon_r)^2} \ln \frac{\left(S_{21}\mathrm{dB} + 15.45006 - 0.01467e^{1.25886\epsilon_r}\right)}{-7.19478 - 0.03569e^{1.02146\epsilon_r}} \tag{3}$$

where Δf is the difference between the sensor's unloaded resonant frequency and resonant frequency when the OUT was loaded.

The resonating frequency of the sensor in the unloaded case was 5.25 GHz. Figure 4 shows that the frequency shifted to 4.83 GHz for castor oil, and 5.03 GHz for flaxseed oil. Moreover, the frequency shifted to 4.89 GHz for mustard oil, and 4.95 GHz for olive oil. These results illustrate that the sensor was sensitive enough to induce a reasonable change in the resonant frequency when loaded with the OUT sample.

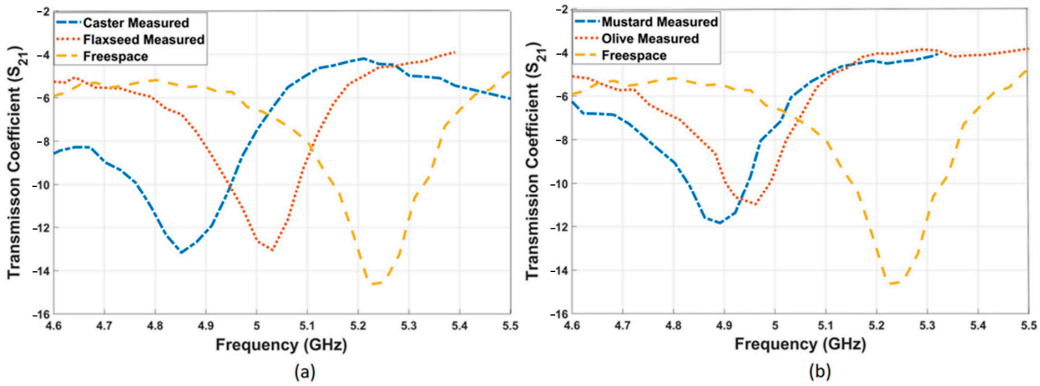

Figure 4. Result of S_{21} for: (**a**) castor and flaxseed oils; (**b**) mustard and olive oils.

A comparison of the shift in resonant frequencies from the reference frequency of 5.25 GHz after the loading of the oil sample, is provided in Table 1. The shift in the frequency was proportional to the permittivity of the OUT.

Table 1. Comparison of shift in frequency for oil samples.

Samples	Frequency (GHz)	Δf (GHz)
Castor oil sim.	4.825	0.405
Castor oil exp.	4.832	0.398
Mustard oil sim.	4.860	0.370
Mustard oil exp.	4.890	0.340
Olive oil sim.	4.952	0.278
Olive oil exp.	4.953	0.277
Flaxseed oil sim.	5.045	0.185
Flaxseed oil exp.	5.030	0.200

From the shift in resonance frequency, and using Equations (2) and (3), permittivity and loss tangent values of OUT were calculated as shown in Table 2. Table 2 shows the retrieved values of the dielectric constants of different oils. The actual values of dielectric constants of these oils could not be found in existing literature at 5.25 GHz. Therefore, at this point, we cannot comment on the accuracy of these values. Table 3 shows the quality factor and sensitivity values for different oil samples. The error column shows the variation of maximum error around the average value after taking multiple measurements for each oil.

Table 2. Permittivity and loss tangent values.

OUT	Dielectric Constant	Loss Tangent	Complex Permittivity	Error
	ϵ	$tan\ \delta$	ϵ''	
Castor oil	4.80	0.03	0.15	±2%
Mustard oil	3.91	0.32	0.12	±1.5%
Olive oil	3.10	0.33	0.10	±1%
Flaxseed oil	2.40	0.03	0.091	±1%
Free-space	1.02	-	-	

Table 3. Sensitivity and quality factor.

OUT	Q-Factor	Sensitivity
	Q	S (%)
Castor oil	39.28	1.9
Mustard oil	37.61	2.1
Olive oil	28.12	3.2
Flaxseed oil	25.15	4.6
Air	-	-

3.3. Sensitivity and Quality Factor

Sensitivity and quality factors are very important sensor parameters. Equations (4) and (6) were used for the calculation of sensitivity and quality factors, where f_c is the center resonance frequency, and f_b is the bandwidth frequency [36]. The bandwidth frequency was obtained using Equation (5).

$$Q = \frac{f_c}{f_b} \tag{4}$$

$$f_b = f_h - f_l \tag{5}$$

where f_h and f_l are higher and lower frequencies at -3 dB of the center frequency, respectively. The sensitivity of the sensor was calculated using Equation (6) [36].

$$S = \frac{f_{empty} - f_{sample}}{f_{empty}\ (\epsilon_r - 1)} \tag{6}$$

where f_{empty} is the unloaded resonant frequency and f_{sample} is the OUT resonant frequency. The highest sensitivity for our sensor was 4.6, whereas the highest quality factor was 39.28.

3.4. Adulteration Detection

After characterization of pure oil, the sensor was validated to detect adulteration in edible oil. For this purpose, pure olive oil was adulterated with castor, argemone, and mustard oil [34]. First of all, as illustrated in Figure 5, 1.5 mL mustard oil was mixed into 15 mL of olive oil, and from this solution, a 1 mL sample was placed directly on the sensor. The resonance frequency shifted from 5.25 GHz to 4.92 GHz. After that, 3 mL of mustard oil was mixed with 15 mL of olive oil, and a 1 mL sample from this solution was placed on the sensor, and the response was measured. In this case, the frequency shifted to 4.86 GHz. The same process was repeated for 4.5 mL of mustard oil in 15 mL olive oil. This time the frequency shifted to 4.69 GHz. Next, samples with 1.5 mL, 3 mL and 4.5 mL of castor oil, in 15 mL of olive oil, were tested. As shown in Figure 5, the frequency shifted to 4.88 GHz, 4.78 GHz and 4.68 GHz, for 1.5 mL, 3 mL and 4.5 mL samples, respectively. Finally, 1.5 mL, 3 mL and 4.5 mL of argemone oil were mixed with samples of 15 mL of olive oil, and the samples from the solutions were tested. Figure 5c shows the S_{21} results for argemone oil as an adulterant. A shift in resonance frequency was clearly visible. Table 4 summarizes the shift in resonance frequency for adulteration detection in different samples of olive oil. The sensor not only detected adulteration, but also differentiated between different levels of adulteration, as seen in Table 4.

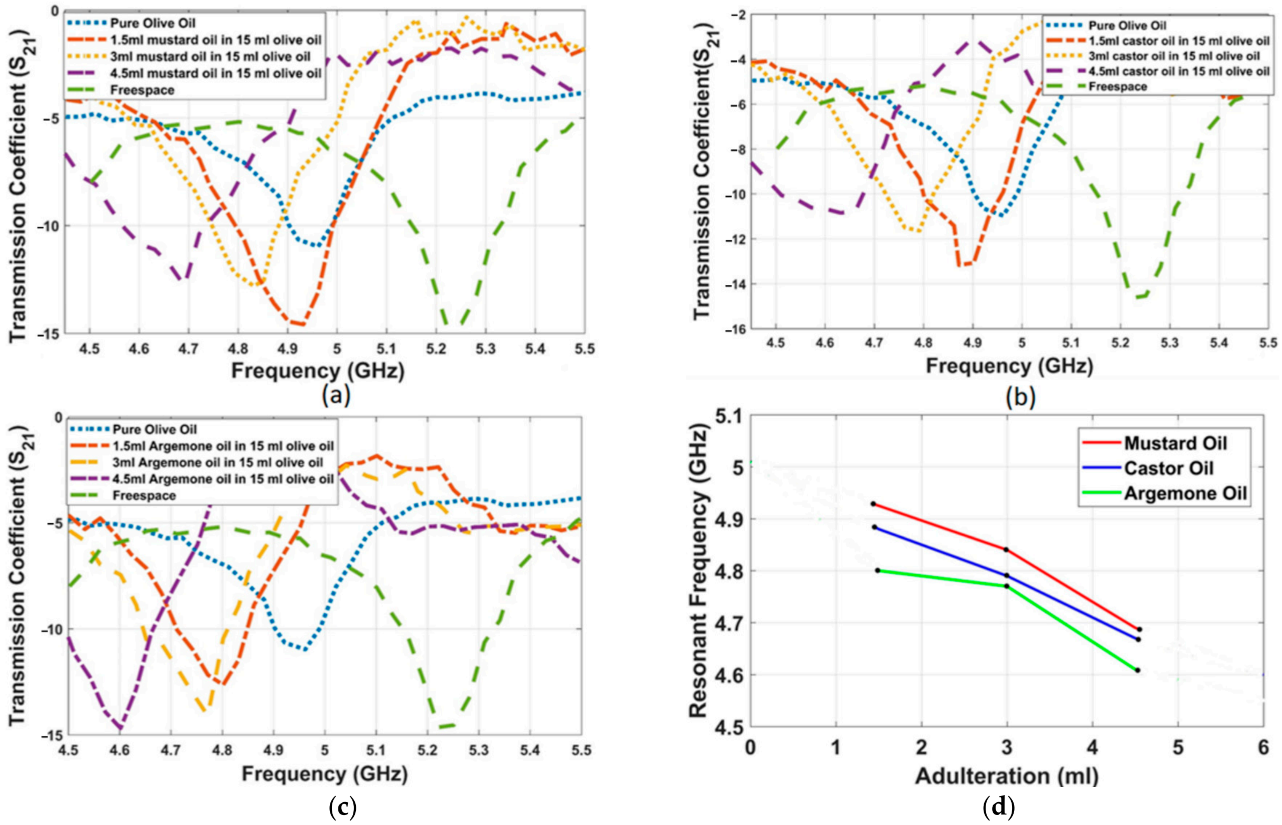

Figure 5. Result of S_{21} after adulteration of mustard oil in olive oil. (**a**) Result of S_{21} after adulteration of mustard oil in olive oil. (**b**) Result of S_{21} after adulteration of castor oil in olive oil. (**c**) Result of S_{21} after adulteration of mustard oil in olive oil. (**d**) Resonant frequency at different values of adulteration.

Table 4. Shift in resonance frequency compared with pure olive oil in different samples.

Sample	Adulteration in Percentage	Resonance Frequency	Shift in Frequency
1.5 mL mustard oil contamination	10%	4.92 GHz	290 MHz
3 mL mustard oil contamination	20%	4.86 GHz	350 MHz
4.5 mL mustard oil contamination	30%	4.69 GHz	520 MHz
1.5 mL castor oil contamination	10%	4.88 GHz	330 MHz
3 mL castor oil contamination	20%	4.78 GHz	430 MHz
4.5 mL castor oil contamination	30%	4.68 GHz	530 MHz
1.5 mL argemone oil contamination	10%	4.80 GHz	400 MHz
3 mL argemone oil contamination	20%	4.78 GHz	430 MHz
4.5 mL argemone oil contamination	30%	4.61 GHz	600 MHz

Table 5 shows the comparative analysis of the proposed sensor with other state-of-the-art RF sensors previously reported in the literature. It is evident that our proposed sensor offers better sensitivity, as well as a better quality factor, on a low-cost substrate, thus, making it a suitable choice for practical applications.

Table 5. Comparison of proposed sensor and other sensor.

Work	Sensitivity	Quality Factor	Structure	Frequency (GHz)	Sensing Area (mm^2)
[33]	0.27	N/A	MTM	2.5	280
[29]	0.05	20	SRR	2.53	124
[37]	0.35	24	Resonator	5.5	344
Our Work	4.6	39	CSRR	5.25	220

4. Conclusions

This research proposed a low-cost, easy-to fabricate, and compact CSRR-based sensor for adulteration detection, as well as characterization, of unpolluted edible oil. The simulated and experimental results of the sensor under oil characteristics and impurities detection were in good agreement. The adulterants were intentionally put in olive oil to measure the shift in frequency peaks. Loss of tangent and relative permittivity were calculated for the given samples of oils. Furthermore, the quality factor and sensitivity values were also obtained for different oil samples. These results suggest that the proposed low-cost sensor can be used for edible oil characterization and adulteration detection in practical applications with high accuracy.

Author Contributions: Conceptualization, M.H.B. and M.A.J.; methodology, M.H.B. and M.A.J.; software, M.H.B., M.A.J. and M.A.K.; validation, M.H.B. and M.A.J.; formal analysis, M.H.B., M.A.J. and M.A.K.; investigation, M.H.B. and M.A.J.; resources, Y.M.; data curation, M.H.B., M.A.J. and M.A.K.; writing—original draft preparation, M.H.B. and M.A.J.; writing—review and editing, M.A.K. and Y.M.; visualization, M.A.K. and Y.M.; supervision, Y.M.; project administration, Y.M.; funding acquisition, Y.M. All authors have read and agreed to the published version of the manuscript.

Funding: The authors would like to acknowledge the research funding to the KAUST Innovative Technologies Laboratories (ITL) from King Abdullah University of Science and Technology (KAUST).

Institutional Review Board Statement: Not applicable.

Informed Consent Statement: Not applicable.

Data Availability Statement: Data underlying the results presented in this paper are not publicly available at this time but may be obtained from the authors upon reasonable request.

Conflicts of Interest: The authors declare no conflict of interest.

References

1. Rahman, N.A.; Zakaria, Z.; Rahim, R.A.; Dasril, Y.; Bahar, A.A.M. Planar Microwave Sensors for Accurate Measurement of Material Characterization: A Review. *TELKOMNIKA (Telecommun. Comput. Electron. Control)* **2017**, *15*, 1108–1118. [CrossRef]
2. Massoud, Y.; Nieuwoudt, A. Modeling and Design Challenges and Solutions for Carbon Nanotube-Based Interconnect in Future High Performance Integrated Circuits. *ACM J. Emerg. Technol. Comput. Syst.* **2006**, *2*, 155–196. [CrossRef]
3. Nieuwoudt, A.; Massoud, Y. Understanding the Impact of Inductance in Carbon Nanotube Bundles for VLSI Interconnect using Scalable Modeling Techniques. *IEEE Trans. Nanotechnol.* **2006**, *5*, 758–765. [CrossRef]
4. Nieuwoudt, A.; Massoud, Y. On the Optimal Design, Performance, and Reliability of Future Carbon Nanotube-Based Interconnect Solutions. *IEEE Trans. Electron Devices* **2008**, *55*, 2097–2110. [CrossRef]
5. Hosseini, A.; Massoud, Y. Optical range microcavities and filters using multiple dielectric layers in metal-insulator-metal structures. *J. Opt. Soc. Am. A* **2007**, *24*, 221–224. [CrossRef]
6. Hosseini, A.; Massoud, Y. A low-loss metal-insulator-metal plasmonic bragg reflector. *Opt. Express* **2006**, *14*, 11318–11323. [CrossRef]
7. Hosseini, A.; Nejati, H.; Massoud, Y. Modeling and design methodology for metal-insulator-metal plasmonic Bragg reflectors. *Opt. Express* **2008**, *16*, 1475–1480. [CrossRef]
8. Hosseini, A.; Nieuwoudt, A.; Massoud, Y. Optimizing Dielectric Strips Over a Metallic Substrate for Subwavelength Light Confinement. *IEEE Photonics Lett.* **2007**, *19*, 522–524. [CrossRef]
9. Muñoz-Enano, J.; Vélez, P.; Gil, M.; Martín, F. Planar Microwave Resonant Sensors: A Review and Recent Developments. *Appl. Sci.* **2020**, *10*, 2615. [CrossRef]
10. Harnsoongnoen, S. Microwave Sensors Based on Coplanar Waveguide Loaded with Split Ring Resonators: A Review. *Appl. Sci. Eng. Prog.* **2019**, *12*, 224–234. [CrossRef]
11. Nyfors, E. Industrial microwave sensors—A review. *Subsurf. Sens. Technol. Appl.* **2000**, *1*, 23–43. [CrossRef]
12. Hosseini, A.; Massoud, Y. Nanoscale surface plasmon based resonator using rectangular geometry. *Appl. Phys. Lett.* **2007**, *90*, 181102. [CrossRef]
13. Hosseini, A.; Nejati, H.; Massoud, Y. Design of a maximally flat optical low pass filter using plasmonic nanostrip waveguides. *Opt. Express* **2007**, *15*, 15280–15286. [CrossRef] [PubMed]
14. Massoud, Y.; Majors, S.; Bustami, T.; White, J. Layout Techniques for Minimizing On-Chip Interconnect Self Inductance. In Proceedings of the 35th IEEE/ACM Design Automation Conference, San Francisco, CA, USA, 15–19 June 1998; pp. 566–571.
15. Massoud, Y.; White, J. Managing On-Chip Inductive Effects. *IEEE Trans. Very Large Scale Integr. (VLSI) Syst.* **2002**, *10*, 789–798. [CrossRef]

16. Zarifi, M.H.; Sohrabi, A.; Shaibani, P.M.; Daneshmand, M.; Thundat, T. Detection of volatile organic compounds using microwave sensors. *IEEE Sens. J.* **2014**, *15*, 248–254. [CrossRef]
17. Massoud, Y.; White, J. Simulation and Modeling of the Effect Substrate Conductivity on Coupling Inductance and Circuit Crosstalk. *IEEE Trans. Very Large Scale Integr. (VLSI) Syst.* **2002**, *10*, 286–291. [CrossRef]
18. Massoud, Y.; Ismail, Y. Grasping the Impact of On-Chip Inductance in High Speed ICs. *IEEE Circuits Devices Mag.* **2001**, *17*, 14–21. [CrossRef]
19. Hosseini, A.; Ragheb, T.; Massoud, Y. A Fault-Aware Dynamic Routing Algorithm for On-Chip Networks. In Proceedings of the 2008 IEEE International Symposium on Circuits and Systems, Seattle, WA, USA, 18–21 May 2008; pp. 2653–2656.
20. Hosseini, A.; Nieuwoudt, A.; Massoud, Y. Efficient simulation of subwavelength plasmonic waveguides using implicitly restarted Arnoldi. *Opt. Express* **2006**, *14*, 7291–7298. [CrossRef]
21. Alam, M.; Massoud, Y. RLC ladder model for scattering in single metallic nanoparticles. *IEEE Trans. Nanotechnol.* **2006**, *5*, 491–498. [CrossRef]
22. Alam, M.; Massoud, Y. A closed-form analytical model for single nanoshells. *IEEE Trans. Nanotechnol.* **2006**, *5*, 265–272. [CrossRef]
23. Massoud, Y.; Kawa, J.; MacMillen, D.; White, J. Modeling and Analysis of Differential Signaling for Minimizing Inductive Cross-Talk. In Proceedings of the 38th IEEE/ACM Design Automation Conference, Las Vegas, NE, USA, 18–22 June 2001; pp. 804–809.
24. Nieuwoudt, A.; Massoud, Y. On the Impact of Process Variations for Carbon Nanotube Bundles for VLSI Interconnect. *IEEE Trans. Electron Devices* **2007**, *54*, 446–455.
25. Javed, A.; Arif, A.; Zubair, M.; Mehmood, M.Q.; Riaz, K. A low-cost multiple complementary split-ring resonator-based microwave sensor for contactless dielectric characterization of liquids. *IEEE Sens. J.* **2020**, *20*, 11326–11334.
26. Massoud, Y.; White, J. Improving the Generality of the Fictitious Magnetic Charge Approach to Computing Inductances in the Presence of Permeable Materials. In Proceedings of the IEEE/ACM Design Automation Conference, New Orleans, LA, USA, 10–14 June 2002; pp. 552–555.
27. Massoud, Y.; White, J. FastMag: A 3-D Fast Inductance Extraction Program for Structures with Permeable materials. In Proceedings of the IEEE/ACM International Conference on Computer Aided Design, San Jose, CA, USA, 10–14 November 2002; pp. 478–484.
28. Massoud, Y.; Alam, M.; Nieuwoudt, A. On the Selection of Spectral Zeros for Generating Passive Reduced Order Models. In Proceedings of the International Workshop on System-on-Chip for Real-Time Applications, Cairo, Egypt, 27–29 December 2006; pp. 160–164.
29. Soffiatti, A.; Max, Y.; Silva, S.G.; de Mendonça, L.M. Microwave metamaterial-based sensor for dielectric characterization of liquids. *Sensors* **2018**, *18*, 1513.
30. Jha, A.K.; Akhtar, M.J. A generalized rectangular cavity approach for determination of complex permittivity of materials. *IEEE Trans. Instrum. Meas.* **2014**, *63*, 2632–2641.
31. Ebrahimi, A.; Scott, J.; Ghorbani, K. Ultrahigh-Sensitivity Microwave Sensor for Microfluidic Complex Permittivity Measurement. *IEEE Trans. Microw. Theory Tech.* **2019**, *67*, 4269–4277.
32. Tiwari, N.K.; Singh, S.P.; Akhtar, M.J. Novel Improved Sensitivity Planar Microwave Probe for Adulteration Detection in Edible Oils. *IEEE Microw. Wirel. Compon. Lett.* **2018**, *29*, 164–166.
33. Muhammed Shafi, K.T.; Jha, A.K.; Akhtar, M.J. Non-destructive technique for detection of adulteration in edible oils using planar RF sensor. In Proceedings of the 2016 IEEE MTT-S International Microwave and RF Conference (IMaRC), New Delhi, India, 5–9 December 2016; pp. 1–4.
34. Kakani, P.N.; Chandu, D.S.; Karthikeyan, S.S. Open complementary split ring resonator based RF sensor with improved sensitivity for detection and estimation of adulteration in edible oils. In Proceedings of the 2019 TEQIP III Sponsored International Conference on Microwave Integrated Circuits, Photonics and Wireless Networks (IMICPW), Tiruchirappalli, India, 22–24 May 2019; pp. 479–482.
35. Baena, J.D.; Bonache, J.; Martin, F.; Sillero, R.M.; Falcone, F.; Lopetegi, T.; Laso, M.A.G.; Garcia-Garcia, J.; Gil, I.; Portillo, M.F.; et al. Equivalent-circuit models for split-ring resonators and complementary split-ring resonators coupled to planar transmission lines. *IEEE Trans. Microw. Theory Tech.* **2005**, *53*, 1451–1461.
36. Alahnomi, R.A.; Zakaria, Z.; Yussof, Z.M.; Althuwayb, A.A.; Alhegazi, A.; Alsariera, H.; Rahman, N.A. Review of recent microwave planar resonator-based sensors: Techniques of complex permittivity extraction, applications, open challenges and future research directions. *Sensors* **2021**, *21*, 2267.
37. Zarifi, M.H.; Rahimi, M.; Daneshmand, M.; Thundat, T. Microwave ring resonator-based non-contact interface sensor for oil sands applications. *Sens. Actuators B Chem.* **2016**, *224*, 632–639.